J Appl Electrochem (2014) 44:325–336
DOI 10.1007/s10800-013-0638-y

RESEARCH ARTICLE

Design and optimization of thermo-electrochemical cells

Pablo F. Salazar · Satish Kumar · Baratunde A. Cola

Received: 23 June 2013 / Accepted: 14 October 2013 / Published online: 22 October 2013

Abstract Thermo-electrochemical cells (or thermocells) convert thermal energy to electricity in continuous operation based on a balance of ion conduction and redox reactions at hot and cold electrodes. In this study, the fundamental governing equations for mass and heat transfer, fluid dynamics, and electrokinetics in thermocells are presented and solved numerically using COMSOL. A parametric study is performed to explore the limitations and optimal cell dimensions for maximum energy conversion efficiency in thermocells. Series-stacking designs are demonstrated to have the potential to increase conversion efficiency by 100 % compared to a single cell configuration. Natural convection is shown to significantly increase the conversion efficiency of thermocells with conventional aqueous electrolyte (0.4 M potassium ferri/ferrocyanide), by compressing the diffusive boundary layers. A flow cell thermocell design is also considered. Results reveal that the ohmic resistance of the electrolyte limits the energy conversion efficiency of this design.

Keywords Thermogalvanic · Thermocells · Flow cell · Series stacking · Multiphysics modeling

List of symbols

A	Electrode surface area (m^2)
β_{T1}	Temperature density change coefficient 1 ($kg\ m^{-3}$)
β_{T2}	Temperature density change coefficient 2 ($kg\ m^{-3}\ K^{-1}$)
β_{T3}	Temperature density change coefficient 3 ($kg\ m^{-3}\ K^{-2}$)
C_p	Electrolyte heat capacity ($J\ kg^{-1}\ K^{-1}$)
C_i	Ion concentration ($mol\ m^{-3}$)
C_i^*	Initial ion concentration ($mol\ m^{-3}$)
C_O	Oxidized concentration ($mol\ m^{-3}$)
C_R	Reduced concentration ($mol\ m^{-3}$)
C_{CI}	Counter-ion concentration ($mol\ m^{-3}$)
D_i	Ion diffusion coefficient ($m^2\ s^{-1}$)
D_O	Oxidized diffusion coefficient ($m^2\ s^{-1}$)
D_R	Reduced diffusion coefficient ($m^2\ s^{-1}$)
D_{CI}	Counter-ion diffusion coefficient ($m^2\ s^{-1}$)
ρ	Electrolyte density ($kg\ m^{-3}$)
ρ_o	Electrolyte density reference at 300 K ($kg\ m^{-3}$)
ε	Dielectric constant ($A^2\ s^4\ kg^{-1}\ m^{-3}$)
E	Electrode potential (V)
E°	Standard electrode potential (V)
E_a	Anode potential (V)
E_a^{eq}	Anode equilibrium potential (V)
E_c	Cathode potential (V)
E_c^{eq}	Cathode equilibrium potential (V)
Ex_a	Rate constant activation energy ($J\ mol^{-1}K^{-1}$)
F	Faraday constant ($C\ mol^{-1}$)
h_e	Effective heat transfer coefficient ($W\ m^{-2}\ K^{-1}$)
I_o	Optimum cell current (A)
j	Electronic current density ($A\ m^{-2}$)
j_a	Electronic current density at the anode ($A\ m^{-2}$)
j_c	Electronic current density at the cathode ($A\ m^{-2}$)
J_{sc}	Short-circuit current density ($A\ m^{-2}$)
j_{wc}	Electronic current density without convection ($W\ m^{-2}$)
k	Electrochemical rate constant ($m\ s^{-1}$)

P. F. Salazar (✉) · S. Kumar · B. A. Cola
George W. Woodruff School of Mechanical Engineering,
Georgia Institute of Technology, Atlanta, GA 30332, USA
e-mail: pablo.salazar@gatech.edu

B. A. Cola
School of Materials Science and Engineering, Georgia Institute
of Technology, Atlanta, GA 30332, USA

k^0	Standard rate constant (m s^{-1})
κ_{s}	Electrolyte thermal conductivity (W m^{-1} K^{-1})
κ_{e}	Electrode thermal conductivity (W m^{-1} K^{-1})
$\vec{N}_{\mathrm{i}}$	Ion flux density (mol m^{-2} s^{-1})
$\vec{N}_{\mathrm{O}}$	Oxidized flux density (mol m^{-2} s^{-1})
$\vec{N}_{\mathrm{R}}$	Reduced flux density (mol m^{-2} s^{-1})
$\vec{N}_{\mathrm{CI}}$	Counter-ion flux density (mol m^{-2} s^{-1})
n	Number of electrons transferred (–)
η	Conversion efficiency (%)
η_{i}	Conversion efficiency of intermediate cell (%)
η_{r}	Relative efficiency (%)
ξ_{a}	Anode overpotential (V)
ξ_{c}	Cathode overpotential (V)
P_{e}	Electric power density (W m^{-2})
P_{i}	Electric power of intermediate cell (W)
P_{m}	Maximum electric power density (W m^{-2})
q	Heat flux density (W m^{-2})
q_{wc}	Heat flux density without convection (W m^{-2})
Q_{CI}	Counter-ion heat of transport (J mol^{-1})
Q_{i}	Ion heat of transport (J mol^{-1})
Q_{O}	Oxidized heat of transport (J mol^{-1})
Q_{R}	Reduced heat of transport (J mol^{-1})
R	Gas constant (J mol^{-1}K^{-1})
$\mathcal{R}_T$	Thermocell volume (m^3)
S	Heat generation sources (W m^{-3})
T	Temperature (K)
T_{a}	Anode temperature (K)
T_{c}	Cathode temperature (K)
T_{H}	Temperature at the hot electrode (K)
T_{o}	Standard temperature (K)
U_{C}	Cold flow temperature (K)
U_{H}	Hot flow temperature (K)
u_{i}	Ion mobility (m^2 s^{-1} V^{-1})
$\vec{u}$	Bulk vector velocity (m s^{-1})
υ	Kinematic viscosity (m^2 s^{-1})
V_{o}	Optimum cell voltage (V)
V_{oc}	Open-circuit cell voltage (V)
V_{T}	Cell voltage (V)
Z_{CI}	Counter-ion charge number (–)
Z_{i}	Ion charge number (–)
Z_{O}	Oxidized charge number (–)
Z_{R}	Reduced charge number (–)
ϕ	Electrostatic potential (V)
θ	Charge transfer coefficient (–)
$\Delta\phi^{\mathrm{s}}$	Solution ohmic drop (V)
$\Delta S^{\circ}_{\mathrm{rx}}$	Standard electrochemical redox reaction entropy (J mol^{-1} K^{-1})
$\Delta H^{\circ}_{\mathrm{rx}}$	Standard electrochemical redox reaction enthalpy (J mol^{-1})
$\Delta G^{\circ}_{\mathrm{rx}}$	Standard electrochemical redox reaction free energy (J mol^{-1})
$\int_a$	Integral at the anode surface
$\int_c$	Integral at the cathode surface
$\int_T$	Integral in the thermocell

1 Introduction

Harvesting low-temperature waste heat could reduce gas emissions and improve the energy efficiency of industrial plants, vehicles, and residential buildings. Devices that can directly convert waste heat to electricity are attractive because they can be compact and lightweight and thus suitable for small-scale or mobile applications, e.g., vehicle or space heat recovery [1, 2]. In addition, such direct energy conversion devices produce zero gas emissions, are reliable, and require very little maintenance because they have no moving parts.

Thermocells are electrochemical devices that produce a steady electric current under an applied temperature difference between the electrodes. If the sign of the redox reaction entropy is negative, the electrode at higher temperature (hot) is designated as the anode; and the cold electrode as the cathode, and vice versa. The cell, filled with a redox electrolyte in an aqueous, or non-aqueous solution or a solid-state membrane, creates a voltage proportional to the redox reaction entropy of the electrolyte. When connected to a load, current flows through the load in an attempt to reach electrochemical equilibrium. The continuity of electronic current is maintained by a flux of the electrolyte within the cell. At the anode the reduced species are consumed, while they are generated at the cathode. The concentration gradient built up drives a diffusion flux that returns the reduced species to the anode and the oxidized species to the cathode. The transport of ions is also driven by a combination of convection, migration, and thermal diffusion. A steady-state current is maintained as long as the temperature difference persists. Figure 1 highlights the main aspects of thermocells. Thermocells can have an extra advantage over conventional solid-state semiconductor thermoelectrics. If the electrodes are made of flexible material, such as buckypaper [3], the cell can be molded to any waste heat source geometry. This versatility eliminates the need for extra equipment to transfer the waste heat, when compared to organic Rankine cycle or conventional semiconductor thermoelectrics.

First reports on thermocells were focused on the study of thermal diffusive potentials associated with the Soret effect in non-isothermal conditions [4–6]. Agar [7] developed an analytical approximate solution for the transient open circuit in a thermocell, considering the equilibration of the thermal diffusion potential. Later, the research was focused on using different redox electrolytes and analyzing their reaction entropy. In a survey of aqueous and non-aqueous

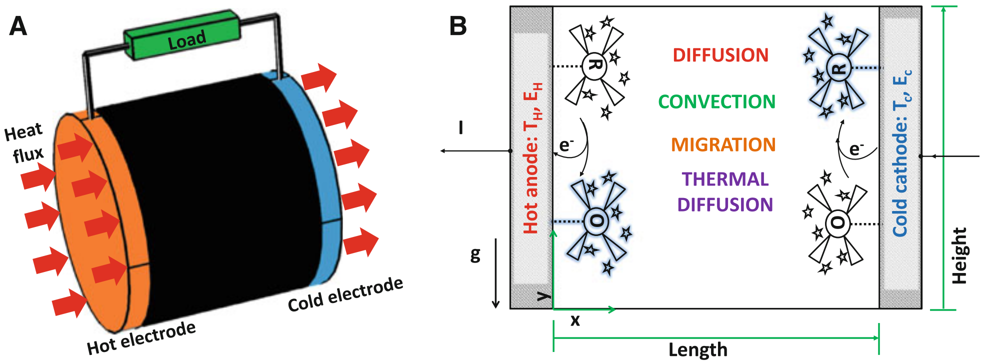

Fig. 1 3D (**a**) and 2D (**b**) schematic representation of thermocells (enclosed cell) with electrodes placed vertically. Cell voltage V_{cell} is a function of the redox reaction entropy, temperature difference at the electrodes and current. Electric current, I, depends on kinetic and mass transfer parameters as well as cell dimensions

electrolytes, aqueous potassium ferri/ferrocyanide solutions were demonstrated to have one of the highest redox reaction entropies, e.g., -180 J mol^{-1} K^{-1} [8]. Conversion efficiencies of <0.1 % and electric powers up to 3 W m^{-2} have been reported for thermocells with aqueous ferri/ferrocyanide solutions and platinum (Pt) electrodes [9–13]. The low efficiencies and the required use of Pt electrodes to achieve kinetic reversibility diminished further research efforts on thermocells since the early studies discussed above. In 2001, Nugent et al. [14] showed fast kinetics using potassium ferri/ferrocyanide on multiwall carbon nanotube (MWCNT) electrodes. Motivated by these results, Hu et al. [3] showed that MWCNT electrodes could be used in thermocells to increase energy conversion efficiency and potentially to reduce their cost as the cost of MWCNTs continues to decrease. Recently, thermocells based on lithium-intercalated electrodes/lithium salts and redox ionic liquids have been demonstrated to have similar thermal-to-voltage conversion values to potassium ferri/ferrocyanide with Pt electrodes [15–17].

Sokirko [18] described an analytical solution for the 1D diffusion–migration transport and 2D diffusion–convection transport in a numerical study of thermocells. Ikeshoji et al. [19, 20] presented a 2D numerical simulation of power, current, and heat flux density considering diffusion, migration, and natural convection in the mass and heat transfer. These reports showed that natural convection has a strong effect in the conversion efficiency of thermocells, because, in low viscosity solutions, mass boundary layers are thinner than thermal boundary layers [10, 18–20]. As consequence, the optimal cell orientation is when vertical electrodes (parallel to gravity) or cold-above hot electrodes are used. However, these simulations were performed considering only a square thermocell of 1 mm side length.

This report seeks to extend the optimization of thermocells to the dimensions and designs of practical cell configurations. In addition, this report highlights the critical limitations on power generation and energy conversion efficiency of current thermocells. We first describe the governing equations of charge, mass and heat transfer for steady-state operation of thermocells. Then, we perform numerical simulations to present the power and conversion efficiency of conventional stagnant thermocells as well as an optimization of cell dimensions. The performance of stacking cells in series is later evaluated. Finally, we estimate the output power of a thermocell design with forced convection of the electrolyte, i.e., a flow cell.

2 Governing equations

2.1 Heat transfer

At steady state, the temperature profile in the electrolyte is governed by

$$\rho C_p \vec{u} \cdot \nabla T = \nabla \cdot \left(\kappa_s \nabla T + \sum D_i Q_i \nabla C_i \right) + S \qquad (1)$$

Heat is transferred to the thermocell from a heat source, e.g., from the surface of a pipe in a power plant with hot water flowing through it. In this report, the anode and cathode are assumed to be at the constant temperature of a waste heat source and the ambient, respectively. An electrolyte with a low thermal conductivity is required to obtain a maximum temperature difference across the electrodes. The maximum operative temperature of thermocells is limited by the boiling point of water in aqueous solutions, or the volatility of the electrolyte in non-aqueous solutions. The minimum operative temperature is set by the solubility of the electrolyte at the cold electrode. The temperature range for optimum performance of aqueous thermocells is between 25 and 75 °C. The second term on the right side of Eq. 1 represents the Dufour effect. The attraction or repulsion of ions to the hot or cold electrode due to the Soret effect leads to an additional heat flux proportional to the diffusivity, concentration gradients, and Soret coefficients of the ions [4, 6]. The last term on the right of Eq. 1, S represents sum of reversible heat due to electrochemical reactions and irreversible heat due to activation overpotentials and Joule heating. As noted by Quickenden and

Mua [12], their contribution in thermocells is relatively small, compared to the conductive–convective heat transfer. The heat produced by these effects is around three orders of magnitude smaller than the heat applied to the thermocells in our model, and it is thus reasonable to neglect them in the model.

2.2 Thermodynamics

A reduction–oxidation (redox) reaction is described as

$$[\mathrm{Reduced}]^{Z_R} \rightleftharpoons [\mathrm{Oxidized}]^{Z_O} + (Z_R - Z_o)[\mathrm{e}^-]. \tag{2}$$

Redox reactions at the electrode are thermodynamically balanced by

$$\Delta G^\circ_{\mathrm{rx}} = \Delta H^\circ_{\mathrm{rx}} - T^\circ \Delta S^\circ_{\mathrm{rx}}. \tag{3}$$

In addition, the standard electrode potential with respect to the standard hydrogen electrode, and the standard reaction free energy are related by

$$E^\circ = \frac{-\Delta G^\circ_{\mathrm{rx}}}{nF}. \tag{4}$$

Formally, concentrations at the electrode surface alter the electrode potential according to the Nernst equation. Thus, the electrode potential at any temperature is [21]

$$E = E^\circ + (T - T^\circ)\frac{\Delta S^\circ_{\mathrm{rx}}}{nF} - \frac{RT}{nF}\ln\frac{C_R}{C_O}. \tag{5}$$

Enthalpy and entropy of reaction can be assumed constant in the temperature range of aqueous solutions.

When the cell is in open circuit or not connected to a load, the initial bulk concentrations are the same as those at the electrode surface. Conventionally, the ratio of oxidized and reduced species is 1. Also, electrolyte reacting at the anode and cathode is the same in thermocells. If the standard electrode potential is independent of the electrode material, which is usually the case for redox couples used in thermocells, we obtain the thermal-to-voltage conversion

$$V_{\mathrm{oc}} = E_c - E_a = -\frac{\Delta S^\circ_{\mathrm{rx}}(T_a - T_c)}{nF}. \tag{6}$$

Hupp and Weaver [8] reported values of standard redox reaction entropy for electrolytes as well as their respective standard electrode potentials. It was found that the reaction entropy is negative, if the absolute charge of the reduced ion is larger than that of oxidized ion. The same publication reports the redox reaction entropy dependence on physicochemical parameters such as oxidation state, metal-atom radius, and solvent molecules. The redox reaction entropy has not been reported to depend on the choice of electrode material.

2.3 Electrode kinetics

A simple expression for the electrode transfer rate constant is [22]

$$k = Z_e \mathrm{e}^{-\frac{Ex_a}{RT}}, \tag{7}$$

where Z_e is a constant frequency factor and Ex_a is the total activation energy fit from the experimental values.

The Butler–Volmer model describes the net electric current densities at the electrodes as [22]

$$j_a = nFk^\circ \exp\left[\frac{Ex_a}{R}\left(\frac{1}{T^\circ} - \frac{1}{T_a}\right)\right]\left[C^a_o \exp\left(\frac{-nF(1-\theta)\xi_a}{RT_a}\right) - C^a_R \exp\left(\frac{nF\theta\xi_a}{RT_a}\right)\right], \tag{8a}$$

at the anode; and

$$j_c = nFk^\circ \exp\left[\frac{Ex_a}{R}\left(\frac{1}{T^\circ} - \frac{1}{T_c}\right)\right]\left[C^c_o \exp\left(\frac{-nF(1-\theta)\xi_c}{RT_c}\right) - C^c_R \exp\left(\frac{nF\theta\xi_c}{RT_c}\right)\right], \tag{8b}$$

at the cathode.

The overpotential, ξ, is the electrode potential with respect to its equilibrium value, which was given in Eq. 6. Therefore, the anode and cathode overpotentials are

$$\xi_a = E_a - E^{\mathrm{eq}}_a, \tag{9a}$$

$$\xi_c = E_c - E^{\mathrm{eq}}_c. \tag{9b}$$

Equation 8a, 8b shows the dependence of these overpotentials on the concentration at the electrode surface and the rate constant k^{o}. The two contributions are defined as activation and concentration overpotentials. The activation overpotential is the overpotential when no mass transfer resistances appear, that is, the concentration at the surface is the same as in the bulk. The concentration overpotential is the actual concentration discrepancy at the surface. Electronic current continuity is satisfied by

$$\int_a j_a \mathrm{d}A = -\int_c j_c \mathrm{d}A. \tag{10}$$

The double layer effect in the electrochemical kinetics requires further clarification. The effective overpotential that applies to the electrode kinetics of Eq. 8a, 8b is lower than that specified by Eq. 8a, 8b because part of the overpotential difference is dissipated in a diffusive layer next to the reaction zone. However, as pointed out by Bockris [23], at high concentrations (above 0.1 M) the diffusive layer is so compact that most of the interphase potential affects the reaction zone only. Thus, the validity of Eqs. 8a, 8b, 9a, and 9b is retained for thermocells.

2.4 Mass transfer

Electric current at the electrodes must be maintained by a flux of ions in the thermocell. The ionic density fluxes for the oxidized and reduced species, and the counter ions are [18]

$$\vec{N}_{\mathrm{O}} = \underbrace{-D_{\mathrm{O}}\nabla C_{\mathrm{O}}}_{\text{diffusion}} - \underbrace{Z_{\mathrm{O}}u_{\mathrm{O}}FC_{\mathrm{O}}\nabla\phi}_{\text{migration}} - \underbrace{\frac{Q_{\mathrm{O}}}{RT^2}D_{\mathrm{O}}C_{\mathrm{O}}\nabla T}_{\text{thermaldiffusion}} + \underbrace{C_{\mathrm{O}}\vec{u}}_{\text{convection}}\ , \tag{11a}$$

$$\vec{N}_{\mathrm{R}} = -D_{\mathrm{R}}\nabla C_{\mathrm{R}} - Z_{\mathrm{R}}u_{\mathrm{R}}FC_{\mathrm{R}}\nabla\phi - \frac{Q_{\mathrm{R}}}{RT^2}D_{\mathrm{R}}C_{\mathrm{R}}\nabla T + C_{\mathrm{R}}\vec{u}, \tag{11b}$$

$$\vec{N}_{\mathrm{CI}} = 0 = -D_{\mathrm{CI}}\nabla C_{\mathrm{CI}} - Z_{\mathrm{CI}}u_{\mathrm{CI}}FC_{\mathrm{CI}}\nabla\phi - \frac{Q_{\mathrm{CI}}}{RT^2}D_{\mathrm{CI}}C_{\mathrm{CI}}\nabla T + C_{\mathrm{CI}}\vec{u} \tag{11c}$$

The thermal diffusion, also known as the Soret effect, represents the ionic flux driven by a thermal gradient, generally from the hot to the cold side [4, 6]. The Nernst–Einstein relationship is used to describe the mobility of ions

$$u_{\mathrm{i}} = \frac{D_{\mathrm{i}}FZ_{\mathrm{i}}}{RT}. \tag{12}$$

Equation 11a, 11b, 11c is strictly valid for only infinitely dilute solutions. Under this approximation, the ion–ion interactions in the bulk are neglected and the activity values become equivalent to concentrations. Following the electrochemical literature, Eq. 11a, 11b, 11c is applied here to thermocells because of its simplicity. Experimental diffusion data at high concentrations is used in an attempt to account for the discrepancy. The electrical neutrality condition

$$\frac{\nabla^2\emptyset}{-F/_{\varepsilon}} = \sum Z_{\mathrm{i}}C_{\mathrm{i}} = 0, \tag{13}$$

is applied in light of the large value of the ratio of F to ε in aqueous solutions [24].

Following the electrochemical reaction stoichiometry at the electrode

$$\vec{N}_{\mathrm{O}}\cdot\vec{n} = -\vec{N}_{\mathrm{R}}\cdot\vec{n}, \tag{14}$$

where $\vec{n}$ is a normal unit vector perpendicular to the electrode. Whereas at the electrically insulated walls, $\vec{N}_{\mathrm{i}}\cdot\vec{n} = 0$ is applied. For every oxidation reaction at the hot electrode, a reduction happens at the cold electrode. Therefore, the total amount of reactants in the cell remains constant. This balance condition is expressed as

$$\int_T C_{\mathrm{i}}\mathrm{d}\mathcal{R}_{\mathrm{T}} = \mathcal{R}_{\mathrm{T}}C_{\mathrm{i}}^{*}. \tag{15}$$

Continuity at the electrodes is satisfied by the balance of ionic and electronic current density

$$j = \sum F\left(Z_{\mathrm{R}}\vec{N}_{\mathrm{R}} + Z_{\mathrm{O}}\vec{N}_{\mathrm{O}}\right)\cdot\vec{n}. \tag{16}$$

There are no homogeneous reactions in the electrolytes conventionally used in thermocells. Thus, at steady state, $\nabla\cdot\vec{N}_{\mathrm{i}} = 0$.

The resultant cell voltage is [22]

$$V_{\mathrm{T}} = V_{\mathrm{oc}} - \xi_{\mathrm{a}} - \xi_{\mathrm{c}} - \Delta\phi^{\mathrm{s}}. \tag{17}$$

2.5 Navier–Stokes equations for fluid flow

The mass conservation equation at steady state is

$$\nabla\cdot(\rho\vec{u}) = 0. \tag{18}$$

In thermocells, density variations with temperature (β_{T1}, β_{T2}) of the form

$$\rho = \beta_{\mathrm{T1}} + \beta_{\mathrm{T2}}T - \beta_{\mathrm{T3}}T^2 \tag{19}$$

are used here [20, 25]. We have omitted density changes due to electrolyte concentration because they represent a small contribution compared to temperature variations [18].

Steady-state momentum conservation in a laminar flow, when only gravitational forces are present, is described as

$$(\vec{u}\cdot\nabla)\vec{u} = \upsilon\nabla^2\vec{u} + \vec{g}\left(\frac{\rho_{\mathrm{o}}-\rho}{\rho_{\mathrm{o}}}\right). \tag{20}$$

Following the Boussinesq approximation, density changes are only considered in terms that contain gravity in the momentum conservation equations. The no-slip condition ($\vec{u} = 0$) is applied at every wall.

2.6 Energy conversion efficiency

Finally, the conversion efficiency of thermocells is evaluated by

$$\eta\,[\%] = \frac{\text{Maximumelectricpower}}{\text{Input heat}}(100) = \frac{V_{\mathrm{o}}I_{\mathrm{o}}}{h_{\mathrm{e}}\Delta T}(100), \tag{21}$$

and the relative efficiency with respect to the Carnot efficiency, $\eta_{\mathrm{r}} = \frac{\eta}{\Delta T/_{T_{\mathrm{H}}}}$. The input heat can be represented by the temperature difference (ΔT) and an effective heat transfer coefficient, h_{e}, which depends on the electrolyte thermal conductivity, cell thickness and, in some cases, natural or forced convection. Since the electric current depends on the cell voltage (based on the Butler–Volmer model), the maximum power is found by optimizing the current and voltage of the cell. The electric current also depends on the effective surface area of the electrode, the effective diffusivity of the ions, the electro-kinetic rate constant, cell thickness, and the effect of natural or forced convection (if there is any).

Table 1 Parameters used in the stagnant thermocell simulation with potassium ferri/ferrocyanide as electrolyte

Parameter (Units)	Value
Cell height (mm)	1
Cell length (mm)	1
Electrolyte heat capacity (J kg^{-1} K^{-1}) [20]	$C_p = 4{,}187$
Initial $K_3Fe(CN)_6$ concentration (mol m^{-3})	400
Initial $K_4Fe(CN)_6$ concentration (mol m^{-3})	400
Density (kg m^{-3}) [25][a]	$1{,}063 + 0.546T - 0.00147T^2$
Diffusion coefficient (m^2 s^{-1}) [25][b]	$(62.66 - 0.5336T + 1.1482 \times 10^{-3}T^2) \times 10^{-10}$
Electrolyte density reference at 300 K (kg m^{-3}) [25][a]	$\rho_o = 1{,}094.6$
Rate constant activation energy (kJ mol^{-1}) [29]	$Ex_a = 14.644$
Charge transfer coefficient [30]	$\theta = 0.5$
Electrode thermal conductivity (W m^{-1} K^{-1})[c]	70
Electrode thickness (mm)	0.1
Side wall thermal conductivity (W m^{-1} K^{-1})[c]	0.05
Side wall insulation thickness (mm)	0.1
Standard rate constant (m s^{-1}) [30][d]	$k^o = 0.6e{-5}$
Electrolyte thermal conductivity (W $m^{-1}K^{-1}$) [20]	$\kappa_s = 0.6$
Number of electrons transferred [29]	$n = 1$
Anode temperature (K)	$T_a = 360$
Cathode temperature (K)	$T_c = 300$
Kinematic viscosity [cm^2 s] [25]	$\nu = \exp\left(-4.818 - 1808T^{-1} + 5.616e5T^{-2}\right)$
Thermal-to-voltage conversion (mV K^{-1}) [26]	1.5

[a] In lack of reported values at 0.4 M, the electrolyte density at 0.2 M was used

[b] The diffusion coefficients and their temperature dependence of the oxidized and reduced species were assumed equal. In lack of reported values at 0.4 M, the diffusion coefficient at 0.2 M was used

[c] The thermal properties of platinum and polystyrene were taken

[d] The rate constant reported at 0.4 M was used

3 Simulation results and discussion

3.1 Conventional thermo-electrochemical cells

A comprehensive model that couples the mass and heat transfer, electrode kinetics, and fluid flow was developed in COMSOL Multiphysics®. This section provides quantitative insights of the output electrical power and heat needed in convectional thermocells, as well as, the upper limits in efficiencies of an optimized cell. Conventional thermocells do not employ forced convection, thus bulk flow of electrolyte is only buoyancy driven. Conventional thermocells use an equimolar aqueous solution of potassium ferri/ferrocyanide due to its high reaction entropy. The maximum concentration of potassium ferri/ferocyanide used in present study is 0.4 M because this is the solubility limit in the electrolyte. No supporting electrolyte is added since it would reduce the solubility of the redox couple. Platinum or MWCNT is used as electrodes because of their high kinetic reactivity and use in prior experimental work [3, 26]. A 2D model, with the *x*-axis in the direction of diffusion and *y*-axis in the direction of the electrode surfaces, is considered as an approximation of a coin cell design [3]. These designs usually have a thickness of ~1 mm. All parameters used in the simulation are presented in Table 1.

Figure 2a shows the current and power density as a function of the cell voltage. The maximum mean power density is reached near half of the open-circuit potential. Unless specified otherwise, the power density and heat flux density reported in the following simulations are the average along the electrodes. Thus, the term "mean" is omitted. An analysis of the kinetic and mass transfer resistances (Fig. 2b) depicts the cathodic concentration overpotential as the major limitation in conventional thermocells. In other words, the current density is mainly limited by the low ionic diffusion at the cold electrode. As a consequence, there is a greater consumption/generation of oxidized/reduced species at this electrode (Fig. 2c). At high current densities, the electrolyte at the cold electrode is depleted and the current density approaches its limiting value. The reversibility of the electrodes translates into small activation overpotentials compared to the total potential drop (inset in Fig. 2b). Temperature, velocities, and concentration profiles under natural convection due to temperature and concentration gradients are shown in Fig. 2d–f, respectively.

Natural convection compresses the boundary diffusive layer (Fig. 2f), thus increasing the ionic flux density at the electrodes and ultimately the power density, as shown in Table 2. Similarly, this electrolyte recirculation increases the input heat flux needed at the hot electrode to maintain the temperature difference set between the two electrodes.

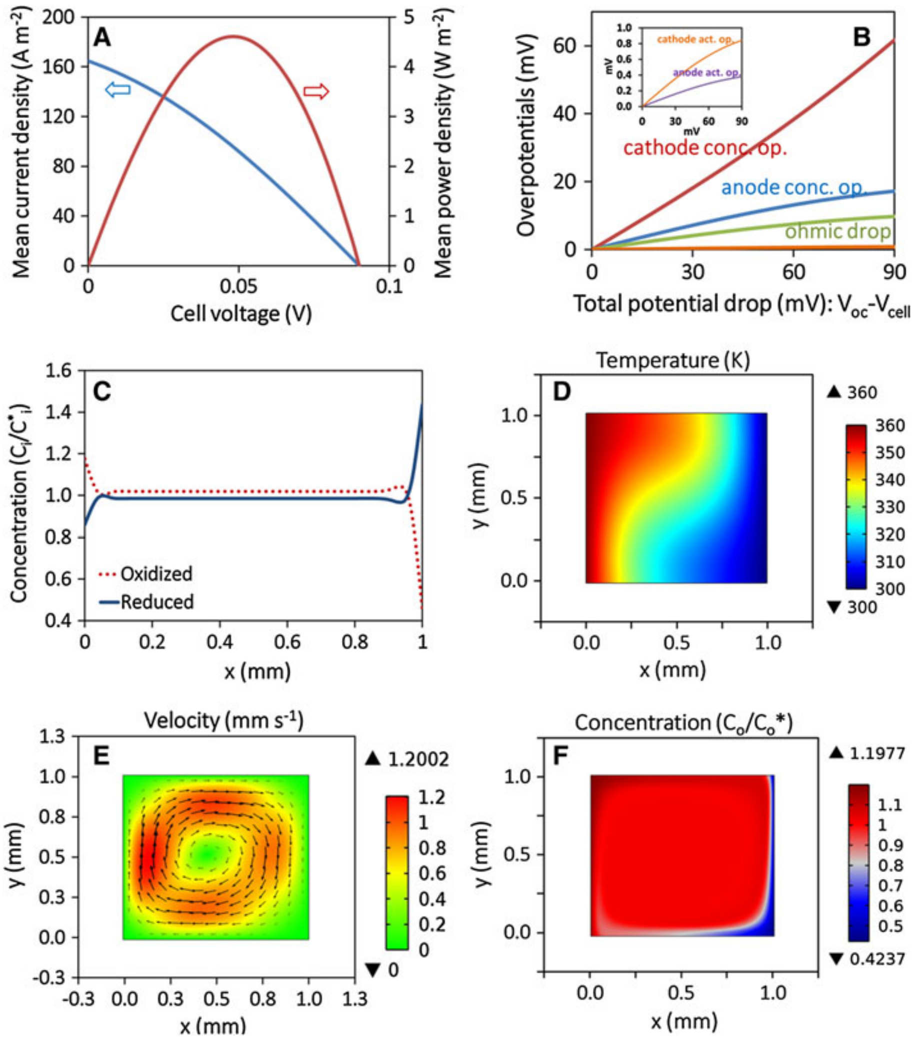

Fig. 2 **a** Current and power density versus cell voltage. **b** Overpotential breakdown (cathode and anode concentration overpotential, and ohmic potential drop; *inset* shows the cathode and anode activation overpotential). **c**–**f** Contour plots at maximum output power for **c** normalized ionic concentration distribution along the center of the cell (y = height/2), **d** temperature (K), **e** velocity (mm s^{-1}) and direction, **f** normalized (with respect to initial concentration) oxidized concentration. Square thermocell of 1 mm length with electrodes placed vertically, anode at the left side (refer to Fig. 1b)

Table 2 Power and heat flux density with and without natural convection included in the simulations with a 1-mm square cell

	With natural convection	Without natural convection
Maximum power density (W m^{-2})	4.61	0.56
Input heat flux density (W m^{-2})	56,050	36,000
Relative efficiency (%)	0.049	0.009

The strength of natural convection on the heat flux density and current density is estimated by the Nusselt and Sherwood number, respectively, [27]

$$\mathrm{Nu} = \frac{q}{q_{\mathrm{wc}}} = 0.667(\mathrm{GrPr})^{0.25},\ \mathrm{Sh} = \frac{j}{j_{\mathrm{wc}}} = 0.667(\mathrm{GrSc})^{0.25}. \tag{22}$$

The fluid is characterized by the Grashof (Gr), Schmidt (Sc), and Prandtl (Pr) number [27]

$$\mathrm{Gr} = \frac{gL^3(\rho_o - \rho)}{v^2\rho_o},\ \mathrm{Sc} = \frac{v}{D},\ \mathrm{Pr} = \frac{v\rho C_p}{\kappa_s}. \tag{23}$$

Combining Eqs. 21–23, the conversion efficiency can then be expressed as

$$\eta[\%] = \frac{V_T \cdot j}{q}(100) = \frac{V_T \cdot j_{\mathrm{wc}} \cdot \mathrm{Sh}}{q_{\mathrm{wc}} \cdot \mathrm{Nu}}(100) = \eta_{\mathrm{wc}} \cdot \left(\frac{\alpha}{D}\right)^{0.25}, \tag{24}$$

$^{\alpha}/_{D}$ ratio is also known as the Lewis (Le) number.

Rayleigh number was at most in the order of 10^7, that is, at least 2 orders of magnitude lower than the critical transition value from laminar to turbulent flow.

For the conditions and cell dimensions given (1-mm square cell), the power density increases 8 times because of natural convection. On the other hand, the input heat flux density at the anode is only 1.5 times higher due to natural convection. The higher power density increase is due to the low diffusion coefficients of redox species in comparison to their thermal diffusivities. The average diffusion coefficient (D) of potassium ferri/ferrocyanide is 4×10^{-10} m^2 s^{-1}, while their thermal diffusivity $\left(\alpha = \frac{\kappa_s}{\rho C_p}\right)$ is 1.4×10^{-7} m^2 s^{-1}. The difference translates into the lack of a temperature boundary

Table 3 Experimental and calculated short-circuit current (J_{sc}) and maximum electric power density (P_m)

Author: Ikeshoji et al. [10] $T_a - T_c = 72$ °C, $T_c = 5.4$ °C, $[K_3Fe(CN)_6] = [K_4Fe(CN)_6] = 0.01$ M, platinum electrodes of 9 mm diameter, electrode separation of 1 mm[a]		
	Exp. P_m (W m^{-2})	Calc. P_m with our model (W m^{-2})
Conductive (hot-above-cold)	0.028	0.03
Conductive-Convective (cold-above-hot)	0.074	0.09
Author: Mua et al. [11] $T_a - T_c = 40$ °C, $T_c = 20$ °C, $[K_3Fe(CN)_6] = [K_4Fe(CN)_6] = 0.26$ M, [KCl] = 0.8 M, platinum electrodes of 1 cm^2 surface area, cold-above-hot electrode configuration[a]		
Electrode distance (cm)	Exp. J_{sc} (A m^{-2})	Calc. J_{sc} with our model (A m^{-2})
0.1	32	38.2
3	14	16.9
5	10	11.8
10	6	7.0
20	3	3.6

[a] The diffusion, rate constant, viscosity, and density parameters at 0.01 M; and the addition of supporting electrolyte was considered in the simulations

layer (Fig. 2c) and a smaller input heat flux increase due to natural convection. Also, the buoyancy effects are due to the temperature gradients rather than by net concentration (oxidized plus reduced species) gradients. The Soret and Dufour effects in aqueous potassium ferri/ferrocyanide solutions were omitted because their relevance on mass and heat transport is relatively small. Heat of transport coefficients of potassium ferri and ferrocyanide in aqueous solutions are about 8.0 kJ mol^{-1} [28].

3.2 Validation

We tested our multiphysics model and the parameters used with experimental values reported by Ikeshoji [10], Mua and Quickenden [11]. In Table 3, we show the dependence of the short-circuit current with the electrode separation for an equimolar potassium ferri/ferrocyanide solution and supporting electrolyte. At electrode separations greater than 1 cm, the electric current is mainly limited by the ohmic resistance of the solution, and the calculated short-circuit current fairly matches the experimental values. We found a higher overestimation of electric current at an electrode separation of 1 mm; i.e., when the transport is driven mainly by conductive and convective forces. The lower experimental short-circuit currents are probably due to the additional boundary layers at the side walls of the cylindrical thermocell, which are not considered in the 2D model. Natural convection can be suppressed by placing the hot electrode above the cold electrode. The experimental and calculated changes of electric power density with the orientation of the cell are shown in Table 3. In addition, the Sherwood and Nusselt numbers for a square thermocell of 1 mm length (Fig. 3a) are in agreement with the computational results of Ikeshoji et al. (Fig. 7 of Ref. [19]). In all simulations, each boundary was meshed with a minimum element size of 2×10^{-7} m (to assure grid independence), linearly distributed from a fine grid near the boundary to a course grid near the center of the cell. The maximum element ratio (the ratio of the biggest and smallest element) was 20. If the minimum element size is decreased to 1×10^{-7} m, the results change <2 %. The simulations converged in <100 iterations with a relative tolerance of 0.001 and using a Multifrontal Massively Parallel sparse direct solver (MUMPS).

3.3 Optimization of cell dimensions

The strength of natural convection with cell aspect ratio (height/length) at a fixed length (1 mm) is depicted in Fig. 3a. At small aspect ratios, convection of heat and mass is small (Nu → 1 and Sh → 1). As aspect ratio increases, convective heat and mass transfer becomes relevant (Sh and Nu increase). An optimum efficiency is found in this transition. Similarly, as the cell length increases, heat conduction decreases and the optimum aspect ratio becomes smaller (Fig. 3b).

Figure 4a shows a non-monotonic change of the relative efficiency as the cell length is increased with the aspect ratio held constant at 1. At small cell lengths, the decrease of power and input heat flux density is linear because conduction and diffusive mass transfer are dominant. The inflection point at 0.1 and 0.5 mm in the power and heat flux density curve, respectively, indicates the compression of boundary layers because of natural convection. The efficiency increases at 0.1 mm because of a secondary effect of temperature gradients in ionic transfer (the

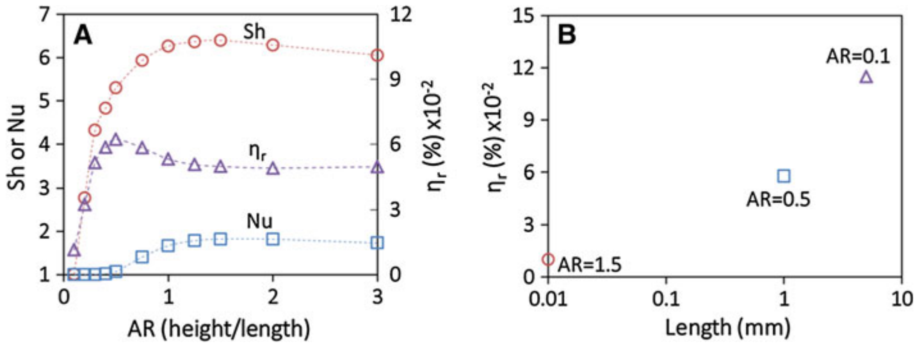

Fig. 3 Effect of aspect ratio (height/length) on natural convection. **a** Sherwood (Sh), Nusselt (Nu), and relative efficiency η_r; cell length fixed at 1 mm. **b** Conversion efficiency and optimum aspect ratio at several cell lengths

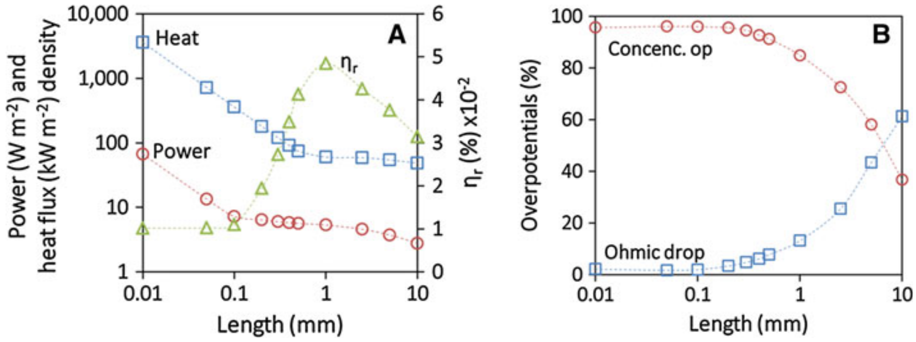

Fig. 4 Cell length parametric study. **a** Maximum power, input heat flux density, and conversion efficiency η_r. **b** Overpotential distribution at maximum power operational points. Aspect ratio held at 1

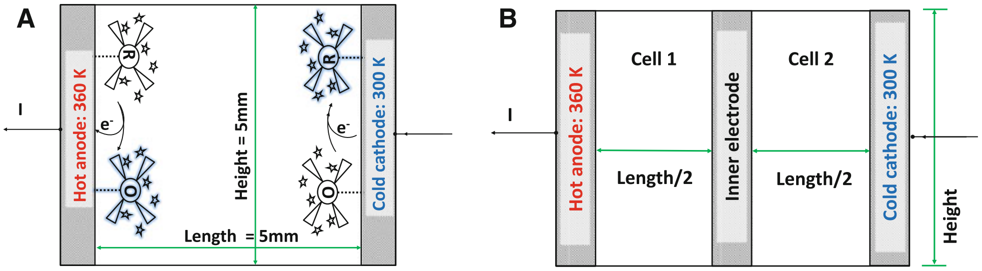

Fig. 5 **a** Schematic representation of stagnant thermocell in a single cell configuration. **b** Example of a series stacking thermocell with two internal cells. The height, total length, temperature of leftmost hot anode and rightmost cold cathode are kept same. In a N-series configuration, the single cell is split into N inner cells of equal size. Other parameters remain same as in Table 1

primary effect being natural convection). As shown in Eq. 24, the effect of natural convection on the efficiency is determined by the ratio of thermal and ionic diffusivities, $^{\alpha}/_{D}$ (Lewis number). The diffusion coefficients near the cold electrode boundary layer should be considered in the Lewis number, because cathodic concentration overpotentials limit the current density (Fig. 2b). As the cell length increases, temperature gradients decrease and the average diffusion coefficient at the cathode boundary layer decreases. Thus, convective forces become stronger at the cold electrode. A maximum efficiency is found at 1-mm thermocell length because as the length increases the ohmic potential drop begins to reduce the available cell voltage (Fig. 4b). Convection is the transport of bulk solution which, by electrical neutrality (Eq. 13), has zero net charge. Thus, any forced or free convection would not create a separation of charges between the electrodes and would not reduce the ohmic resistance.

3.4 Series stacking

Implementation of thermocells to waste heat sources would require thicker cells in order to assure a maximum temperature difference. We consider the case of a single cell (5 mm length and 5 mm height) that is split in equal sized cells and stacked in series. In a series configuration stacking as shown in Fig. 5, the input heat flux coming out from the hotter inner cell is transferred to the next inner cell (since the side walls are considered insulated). The total conversion efficiency in a series configuration is then

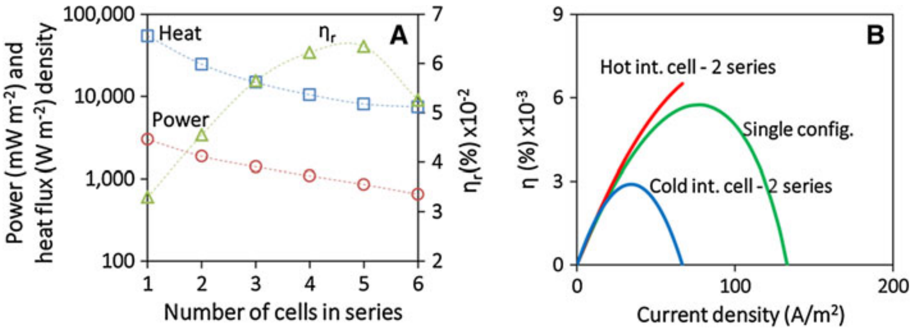

Fig. 6 Series stacking analysis. **a** Relative efficiency, power and input heat flux density in a N-series configuration. Number of cells equal to 1 refers to the single configuration (Fig. 5a). **b** Efficiency breakdown of a 2-series and single configuration

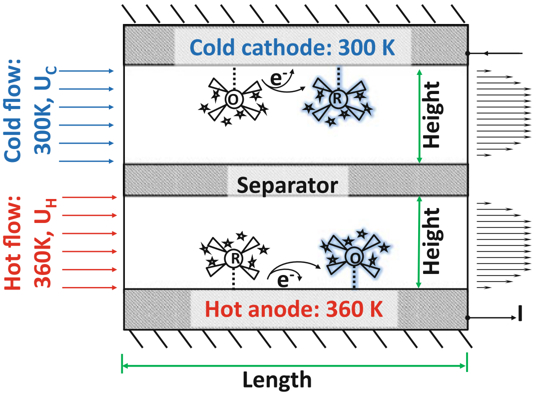

Fig. 7 Schematic representation of a flow-thermocell. Hot and cold compartments are assumed to have a uniform temperature of 360 and 300 K, respectively. Compartment height is 5 mm, and length is 10 mm. Hot and cold inlet equimolar concentration equals 400 mol m^{-3}. Hot and cold flow rate is 0.1 m s^{-1}. Refer to Table 1 for the remaining parameters

$$\eta[\%] = \frac{\sum_{i=1}^{N} P_i}{\text{Heat input}}(100) = \sum\nolimits_{i=1}^{N} \eta_i. \qquad (25)$$

Input heat flux and power density decrease after the cell splitting (Fig. 6a), because the reduced length of the intermediate cells decreases the natural convection in them (Grashof number decreases). Figure 6b shows the efficiency of each intermediate cell in a 2-series stack as well as in the single configuration. The current density of the hotter intermediate cell is discontinued because the limit of the cooler cell is reached. The maximum efficiency in the coupled cell is found by the efficiency sum of the intermediate cells at the same current density. Hotter intermediate cells have higher efficiency because ionic diffusive flux increases as its mean temperature increases, and because the loss of convective forces is less critical in the hotter intermediate cells (high diffusion coefficient and low Sherwood number). However, consecutive cell splitting reduces the limiting current of the colder intermediate cells (low mean temperature) and eventually lowers the efficiency of the stack.

3.5 Flow-thermo-electrochemical cell

Implementation of thermocells in established flows and thermal gradients, like heat exchangers, can result in extra power production that would otherwise be lost. A forced convection or flow-thermocell design is shown in Fig. 7, where a cold and hot equimolar redox electrolyte flow enter the thermocell at a flow rate U_C and U_H, respectively. A no-slip velocity boundary condition is applied at the electrodes and separator walls. The outside walls of the electrodes are insulated. The loss of thermal energy from the chemical reactions and friction through the walls is assumed to be negligible. A uniform cold and hot temperature in the cathode and anode compartments is maintained, respectively. The temperature difference between the electrodes generates a cell voltage proportional to the redox reaction entropy. In a closed circuit, ionic flux, and oxidation and reduction at the electrodes maintains the electric current through the load. Natural convection due to

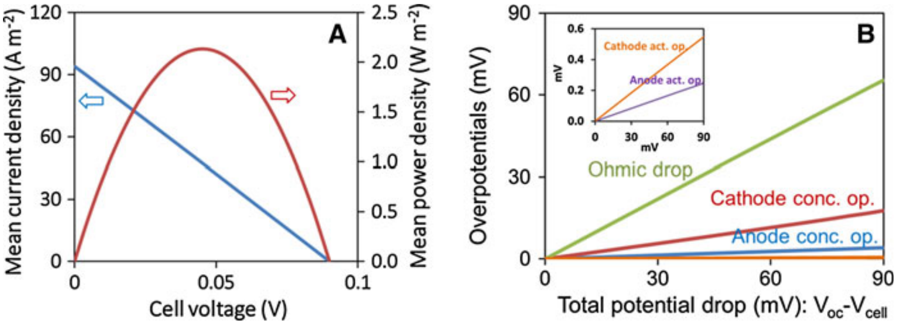

Fig. 8 Performance of a flow-thermocell at 0.1 m s^{-1} inlet electrolyte flow rate. Cell dimensions as described in Fig. 7. **a** Average current and power density versus cell voltage. **b** Breakdown of the overpotential components (ohmic drop, concentration and activation overpotentials)

concentration and temperature gradients is neglected because each compartment (cold and hot) remains almost isothermal. Aqueous potassium ferri/ferrocyanide is used as electrolyte; thus, the Soret and Dufour effects are negligible. Also, the ionic molar resistivity of the membrane has been omitted.

As shown in Fig. 8, the majority of the potential drop in the flow thermocell modeled here is due to the electrolyte resistivity. Consequently, current density changes linearly with cell voltage, which means the current has a strictly ohmic nature. Transient currents due to ionic diffusion in the boundary layer vanish rapidly as reported previously [3]. These results considered along with the dependence of the power on cell length as shown in Fig. 4 suggest that a fundamental limit exist on the ability to scale thermocells, as any form of convection would not improve the performance past a point.

4 Conclusions

This work reveals key features that must be considered in the design of thermocells, and highlights points of performance optimization and limitation. The diffusive boundary layer at the electrodes was shown to limit the current densities of thermocells. Natural convection in conventional thermocells was shown to compress the boundary layers and increase mass and heat transfer depending on their ion diffusivity and thermal diffusivity coefficients, respectively. In conventional thermocells with 1 mm thickness and a temperature difference of 60 °C, natural convection increases mass transfer of the electrolyte by a factor of 8; however, heat flux across the electrodes increases by only a factor of 1.5 due to natural convection. The net effect of natural convection is thus an enhancement of the energy conversion efficiency of thermocells, compared to thermocells with stagnant electrolyte. Although larger cell dimensions could strengthen natural convection, the high ionic resistivity would then limit the output power and efficiency. Numerical results show that series stacking of thermocells increases the overall conversion efficiency by optimizing the impact of natural convection on mass and heat transfer in the individual cells. In a flow cell thermocell design, forced convection lowers the concentration overpotentials; however, the power is limited by the low ionic conductivity of the electrolyte. The ohmic potential drop consumes about 70 % of the open-circuit voltage generated in a flow cell thermocell. Further efficiency improvement of thermocells requires the discovery or synthesis of an electrolyte with high redox reaction entropy and low thermal conductivity to increase the thermal-to-voltage conversion. It should also have high ionic conductivity and fast kinetics at the electrodes to maximize the current density.

Acknowledgments We are grateful for the financial support of National Science Foundation Award No. CBET 1055479.

References

1. Hendricks T, Choate WT (2006) Engineering scoping study of thermoelectric generator systems for industrial waste heat recovery. U.S. Department of Energy, Washington, DC
2. Yang J, Caillat T (2006) Thermoelectric materials for space and automotive power generation. MRS Bull 31(03):224–229. doi:10.1557/mrs2006.49
3. Hu R, Cola BA, Haram N, Barisci JN, Lee S, Stoughton S, Wallace G, Too C, Thomas M, Gestos A, Cruz MEd, Ferraris JP, Zakhidov AA, Baughman RH (2010) Harvesting waste thermal energy using a carbon-nanotube-based thermo-electrochemical cell. Nano Lett 10(3):838–846. doi:10.1021/nl903267n
4. Agar JN (1963) Thermogalvanic cells. In: Delay P, Tobias CW (eds) Advances in electrochemistry and electrochemical engineering, vol 3. Interscience, New York, pp 31–121
5. deBethune AJ (1960) Irreversible thermodynamics in electrochemistry. J Electrochem Soc 107(10):829–842
6. Tyrrell HJ (1961) Diffusion and heat flow in liquids. Butterworths, London
7. Agar JN (1960) The rate of attainment of Soret equilibrium. Trans Faraday Soc 56:776–787
8. Hupp JT, Weaver MJ (1984) Solvent, ligand, and ionic charge effects on reaction entropies for simple transition-metal redox couples. Inorg Chem 23(22):3639–3644. doi:10.1021/ic00190a042
9. Chum HL, Osteryoung RA (1981) Review of thermally regenerative electrochemcial systems, vol 1–2. U.S. Department of Energy, Washington, DC
10. Ikeshoji T (1987) Thermoelectric conversion by thin-layer thermogalvanic cells with soluble redox couples. Bull Chem Soc Jpn 60(4):1505–1514. doi:10.1246/bcsj.60.1505
11. Mua Y, Quickenden TI (1996) Power conversion efficiency, electrode separation, and overpotential in the ferricyanide/ferrocyanide thermogalvanic cell. J Electrochem Soc 143(8):2558–2564. doi:10.1149/1.1837047
12. Quickenden TI, Mua Y (1995) A review of power generation in aqueous thermogalvanic cells. J Electrochem Soc 142(11):3985–3994
13. Quickenden TI, Vernon CF (1986) Thermogalvanic conversion of heat to electricity. Sol Energy 36(1):63–72. doi:10.1016/0038-092x(86)90061-7
14. Nugent JM, Santhanam KSV, Rubio A, Ajayan PM (2001) Fast electron transfer kinetics on multiwalled carbon nanotube microbundle electrodes. Nano Lett 1(2):87–91. doi:10.1021/nl005521z
15. Abraham TJ, MacFarlane DR, Pringle JM (2011) Seebeck coefficients in ionic liquids—prospects for thermo-electrochemical cells. Chem Commun 47(22):6260–6262
16. Hudak NS, Amatucci GG (2011) Energy harvesting and storage with lithium-ion thermogalvanic Cells. J Electrochem Soc 158(5):A572–A579. doi:10.1149/1.3568820
17. Migita T, Tachikawa N, Katayama Y, Miura T (2009) Thermoelectromotive force of some redox couples in an amide-type room-temperature ionic liquid. Electrochemistry 77(8):639–641
18. Sokirko AV (1994) Theoretical study of thermogalvanic cells in steady state. Electrochim Acta 39(4):597–609. doi:10.1016/0013-4686(94)80106-1
19. Ikeshoji T, de Nahui FNB, Kimura S, Yoneya M (1991) Computer analysis on natural convection in thin-layer thermocells with a soluble redox couple: Part 2. E-I relation, electric power, heat flux and electrochemical heat pump. J Electroanal Chem 312(1–2):43–56. doi:10.1016/0022-0728(91)85143-d

20. Ikeshoji T, Kimura S, de Nahui FNB, Yoneya M (1991) Computer analysis of natural convection in thin-layer thermocells with a soluble redox couple: Part 1. Method and the unsteady problem. J Electroanal Chem 307(1–2):29–45. doi:10.1016/0022-0728(91)85537-y
21. Newman J (1995) Thermoelectric effects in electrochemical systems. Ind Eng Chem Res 34(10):3208–3216. doi:10.1021/ie00037a005
22. Bard AJ (2001) Electrochemical methods: fundamentals and applications, 2nd edn. Wiley, Hoboken
23. Bockris JOM (1973) Modern electrochemistry: an introduction to an interdisciplinary area vol 2. Plenum Press, New York
24. Newman JS (1991) Electrochemical systems, 2nd edn. Prentice-Hall, Englewood Cliffs
25. Saraç H, Patrick MA, Wragg AA (1993) Physical properties of the ternary electrolyte potassium ferri-ferrocyanide in aqueous sodium hydroxide solution in the range 10–90 °C. J Appl Electrochem 23(1):51–55. doi:10.1007/bf00241575
26. Salazar PF, Kumar S, Cola BA (2012) Nitrogen- and boron-doped carbon nanotube electrodes in a thermo-electrochemical cell. J Electrochem Soc 159(5):B483–B488. doi:10.1149/2.043205jes
27. Pentrice GA (1991) Electrochemical engineering principles. Prentice Hall, Englewood Cliffs
28. Breck WG, Lin J (1965) Thermal diffusion studies with redox electrodes. Part 2. Ferro-ferricyanide couple. Trans Faraday Soc 61:1511–1515
29. Daum PH, Enke CG (1969) Electrochemical kinetics of the ferri-ferrocyanide couple on platinum. Anal Chem 41(4):653–656. doi:10.1021/ac60273a007
30. Spiro M (1964) Standard exchange current densities of redox systems at platinum electrodes. Electrochimica Acta 9(11):1531–1537